STRUCTURE-AIDED DESIGN OF ANTIVIRAL AGENTS

Acta Cryst. (1995). D**51**, 473–489

Binding of the Antiviral Drug WIN51711 to the Sabin Strain of Type 3 Poliovirus: Structural Comparison with Drug Binding in Rhinovirus 14

BY CHAITANYA N. HIREMATH, ROBERT A. GRANT AND DAVID J. FILMAN

Department of Biological Chemistry and Molecular Pharmacology, Harvard Medical School, Boston, MA 02115, *USA*

AND JAMES M. HOGLE*

Department of Biological Chemistry and Molecular Pharmacology, Harvard Medical School, Boston, MA 02115, *USA, and Committee for Higher Degrees in Biophysics, Harvard University, Cambridge, MA* 02138, *USA*

(*Received* 1 *June* 1994; *accepted* 20 *September* 1994)

Abstract

The crystal structure of the Sabin strain of type 3 poliovirus (P3/Sabin) complexed with the antiviral drug WIN51711 has been determined at 2.9 Å resolution. Drugs of this kind are known to inhibit the uncoating of the virus during infection, by stabilizing the capsid against receptor-induced conformational changes. The electron density for the bound drug is very well defined so that its position and orientation are unambiguous. The drug binds in a nearly extended conformation, slightly bent in the middle, in a blind pocket formed predominantly by hydrophobic residues in the core of the β-barrel of capsid protein VP1. Comparisons between this structure, the corresponding drug complex in human rhinovirus 14 (HRV14), and the native structures of both viruses demonstrate that the binding of WIN51711 has markedly different effects on the structures of these two viruses. Unlike HRV14, wherein large conformational changes are observed in the coat protein after drug binding, the binding of this drug in poliovirus does not induce any significant conformational changes in the structure of the capsid protein, though the drug has a greater inhibitory effect in P3/Sabin than in HRV14. The implications of this result for the mechanism of capsid stabilization are discussed.

Introduction

Picornaviruses are small non-enveloped icosahedral viruses composed of 60 copies each of four capsid proteins, VP1, VP2, VP3 and VP4, surrounding one copy of a single-stranded plus-sense RNA genome. Polio-, rhino-, foot and mouth disease, coxsackie-, cardio- and hepatitis A viruses are all members of the picornavirus family. Polioviruses are the causative agents of poliomyelitis and rhinoviruses are major causes of the common cold in humans. The three-dimensional structures of several strains of poliovirus and rhinovirus have been solved (Hogle, Chow & Filman, 1985; Filman *et al.*, 1989; Yeates *et al.*, 1991; Rossmann *et al.*, 1985; Kim *et al.*, 1989; Oliveira *et al.*, 1993) and all are very similar.

In the course of infecting a cell, picornavirions are required to undergo a series of extensive conformational changes which result in the externalization and/or release of components of the protein shell which are entirely internal in the native virion (Fricks & Hogle, 1990). Later, less well understood stages of this process lead to the release of the viral RNA across the cytoplasmic or endosomal membrane, into the host cell cytoplasm. This sequence of conformational alterations is designed to be triggered by the binding of virus to specific host cell receptors. However, similar non-productive changes in virion structure can be induced by a variety of chemical and physical influences (notably high temperature), leading to the irreversible inactivation of the virus (LeBouvier, 1959; Roizman, Mayer & Roane, 1959; Hummler Anderson & Brown, 1962; Katagiri, Hinuma & Ishida, 1967). Thus, finding a means to stabilize the virion structure (at ambient and physiological temperatures) offers both the possibility of preventing infection by inhibiting the uncoating process, and the possibility of stabilizing live vaccine stocks against thermal inactivation.

The structural integrity of the native picornavirion can be stabilized by several protective factors, including various salts (Wallis & Melnick, 1961), sucrose, lysine and other diamines (Dorval, Chow & Klibanov, 1990), and short-chain fatty acids (Ismail-Cassim, Chezzi & Newman, 1990, Dorval *et al.*, 1990). The uncoating of poliovirus and human rhinoviruses can be inhibited by treating the virion with certain antiviral agents (Fox, Otto, McKinlay, 1986) such as those made by Sterling-Winthrop Pharmaceutical Research Division (WIN com-

* Author for correspondence.

Table 1. *Dihedral angles (°) of compounds binding to polio- and rhinoviruses*

Torsion about	WIN51711 in P3/Sabin	Spingosine in P3/Sabin	Palmitate in V510	WIN51711 in HRV14
a	178	176	175	−124
b	179	176	167	−170
c	55	62	58	140
d	−180	174	144	101
e	167	175	166	96
f	−175	−174	171	120
g	161	−180	174	127
h	−177	−174	−163	174
i	−112	−68	−112	−6

pounds) (Fox *et al.*, 1986; Woods *et al.*, 1989; Diana *et al.*, 1989) and by Janssen Research Foundation (Al-Nakib *et al.*, 1989; Andries *et al.*, 1992) (Fig. 1, Table 1). These compounds have been shown to stabilize the capsid against denaturation caused by heat and extremes of pH (McSharry, Caliguiri & Eggers, 1979; Caliguiri, McSharry & Lawrence, 1980), and also inhibit the attachment of virus to receptors on the outer surface of susceptible cells in certain strains of rhinovirus (Pevear *et al.*, 1989).

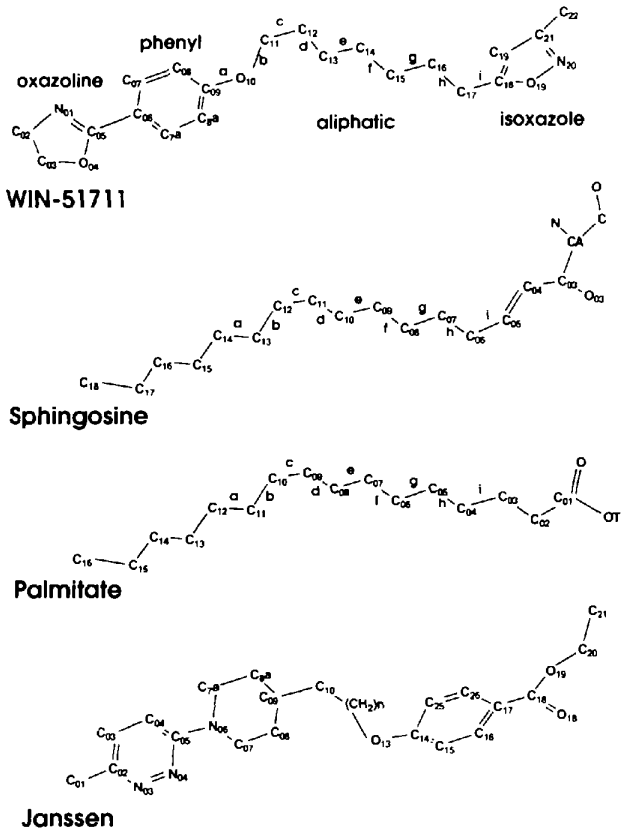

Fig. 1. Chemical structures and bound conformations of some compounds which bind at the center of the VP1 β-barrel in certain polioviruses and rhinoviruses. The conformations of WIN51711 and sphingosine as shown are similar to those observed in complexes with the P3/Sabin. The conformation of palmitate was seen in the chimeric poliovirus V510 (Yeates *et al.*, 1991). Conformations are not indicated for the series of compounds (n = 1, 2 and 3) from Janssen Pharmaceuticals. Lower case letters identify specific dihedral angles. See Table 1 for values of these angles.

Crystallographic studies of native polioviruses (Hogle *et al.*, 1985; Filman *et al.*, 1989) demonstrated that the hydrophobic core of the β-barrel of major capsid protein VP1 is occupied by a natural ligand. This is a narrow molecule, in a generally extended conformation, but bent in the middle. Its more deeply buried end makes exclusively hydrophobic contacts with C atoms from the side chains of hydrophobic amino-acid residues, while its open end is in contact with polar groups and with solvent. The binding pocket for this ligand connects with the outer surface of the virus through a pore. No such ligand was observed in the analogous site in the crystal structure of native rhinovirus 14 (Rossmann *et al.*, 1985). Although no direct chemical identification of the natural ligand has proved to be possible, model-building exercises (in the context of the distribution of hydrogen-bonding groups in the protein) made sphingosine an attractive candidate for the ligand (Fig. 1). However, the electron density for the head-group region of the molecule is weak and occupancy of the pocket by a mixture of lipids could not be ruled out. In subsequent crystallographic studies of a variety of poliovirus strains (Filman *et al.*, 1989; Yeates *et al.*, 1991), and of an assembly intermediate (Basavappa *et al.*, 1994) every structure has contained an analogous naturally occurring ligand. In most cases the shape of the density and the distribution of potential hydrogen-bond donors and acceptors have been consistent with the earlier identification of sphingosine as a possible ligand. In some strains and mutants, the shape of the electron-density feature and the hydrogen-bonding pattern have suggested that palmitate (Fig. 1) or a shorter fatty acid is bound instead (Yeates *et al.*, 1991; Jacobson, Hogle & Filman, 1995).

The crystal structures of native rhinovirus 1A (Kim *et al.*, 1989) and rhinovirus 16 (Oliveira *et al.*, 1993) have contained electron-density features in the outer portion of the analogous lipid-binding site which have been modeled as short-chain (seven- or eight-carbon) fatty acids. The term 'pocket factor' (Oliveira *et al.*, 1993) has lately come into common use to refer to the naturally occurring ligand. The biological importance of a structurally conserved lipid-binding pocket in poliovirus and rhinovirus is still not entirely clear, but the necessary interaction of picornaviral capsid proteins with cellular membranes during viral assembly and cell entry, together with the demonstration that mutations within the drug-binding site can affect the thermal stability of assembly intermediates (Macadam, Ferguson, Arnold & Minor, 1991; Filman *et al.*, 1989), has made the biological roles of the pocket (and of its natural ligand) the subject of considerable speculation (Filman *et al.*, 1989; Flore, Fricks, Filman & Hogle, 1990; Oliveira *et al.*, 1993; Mosser & Rueckert, 1993).

A specific role for the pocket in the regulation of capsid stability was first demonstrated by the results of Rossmann and coworkers (Smith *et al.*, 1986; Badger *et al.*, 1988; Badger, Minor, Oliveira, Smith & Rossmann, 1989) showing that a series of antiviral compounds including WIN51711 bind to rhinovirus 14 in a site analogous to the lipid-binding pocket in poliovirus. Comparisons of these virus–drug complexes with the structure of native rhinovirus 14 showed that the binding of these drugs (to rhinovirus 14) caused significant changes in the main-chain conformation of several amino-acid residues in the vicinity of the 'pore'. In particular, residues at the carboxyl end of the '*GH* loop' of VP1, which were normally collapsed into the mouth of the pocket in the absence of drug, were excluded from that conformation by steric conflicts with bound drug. The conformation produced by drug binding was more similar to that seen in native poliovirus, with its natural ligand bound. The Rossmann group inferred that the conformational change produced by drug binding played a direct causative role in the mechanism by which drug binding stabilized virions and prevented uncoating (Smith *et al.*, 1986; Badger *et al.*, 1988; Badger, Minor *et al.*, 1989). More recent studies have further suggested that the observed conformational changes may interfere with the binding of virus by host cell receptors, possibly by locking the virus into a conformation unsuitable for receptor interaction (Oliveira *et al.*, 1993).

Within the past two years, the crystal structures of rhinoviruses 1A and 16 also have been determined in complex with a number of antiviral compounds from Sterling-Winthrop (Kim *et al.*, 1993; Oliveira *et al.*, 1993); and the structures of a number of poliovirus variants were determined in complex with a series of compounds from Janssen Pharmaceuticals (Grant *et al.*, 1994) (see Fig. 1, Table 1). In contrast to the rhinovirus 14 drug complexes, where drug binding was associated with large local conformational changes in capsid protein VP1 in the vicinity of the drug-binding pocket, the polioviruses and rhinovirus 1A and 16 exhibit minimal changes upon drug binding, presumably due to the presence of a natural ligand in their native structures.

In this paper, we report the crystal structure of WIN51711 in complex with the Sabin strain of type 3 poliovirus (P3/Sabin) and compare it with the correspond-

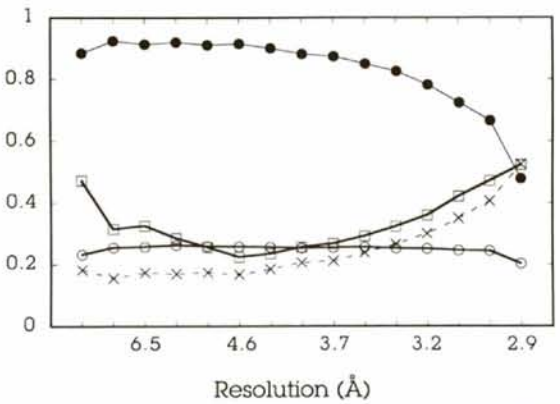

Fig. 2. Agreement statistics for the WIN51711 complex with P3/Sabin as a function of resolution. Reflections from 30 to 2.9 Å were divided into 16 shells of roughly equal reciprocal volume. In each shell open circles represent the completeness of the data (the number of measured reflections as a fraction of the number theoretically possible), closed circles and crosses represent, respectively, the linear correlation coefficient (R_{corr}) and r factor [R(1)nonx], which assess the extent to which the Fourier transform of the non-crystallographic symmetry constrained map (F_{calc}) agrees with the observed structure-factor magnitudes (F_{obsd}). Open squares represent the model-dependent r factor derived from the refined atomic model. $R(1) = [\Sigma_h||F_{obsd}(h)| - K_{bin}|F_{calc}(h)||]/\Sigma_h|F_{obsd}(h)|$ where K_{bin} is a resolution-dependent scale factor.

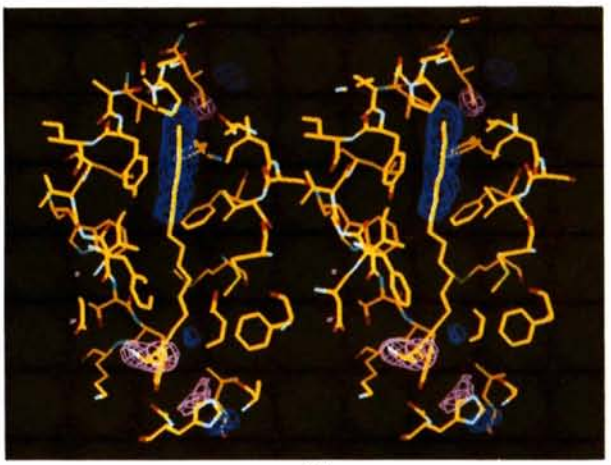

(*a*)

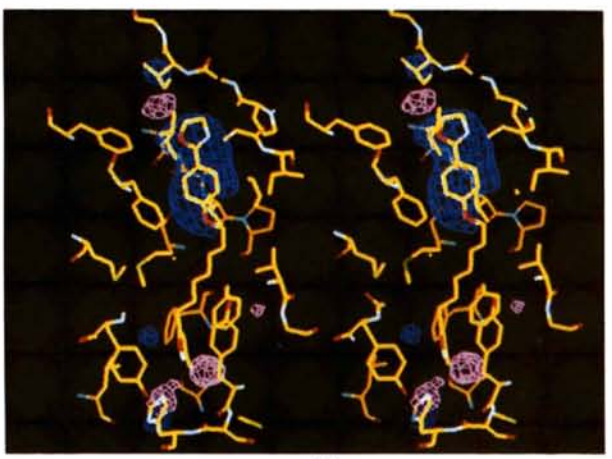

(*b*)

Fig. 3. Stereoviews of the icosahedrally averaged drug-minus-native difference map in the vicinity of the ligand-binding pocket at the center of the VP1 β-barrel of P3/Sabin. Positive difference-density features are drawn in blue and negative features are pink. For greater clarity, portions of the map and model at the front and back of these views have been truncated. (*a*) is a side view of the pocket, from a viewpoint similar to Fig. 5(*a*). Difference density is shown superimposed on a portion of the native P3/Sabin model, which includes bound sphingosine. (*b*) is a top view of the pocket, from a viewpoint similar to Fig. 5(*b*). This panel includes a portion of the atomic model of the P3/Sabin complex with the antiviral compound WIN51711.

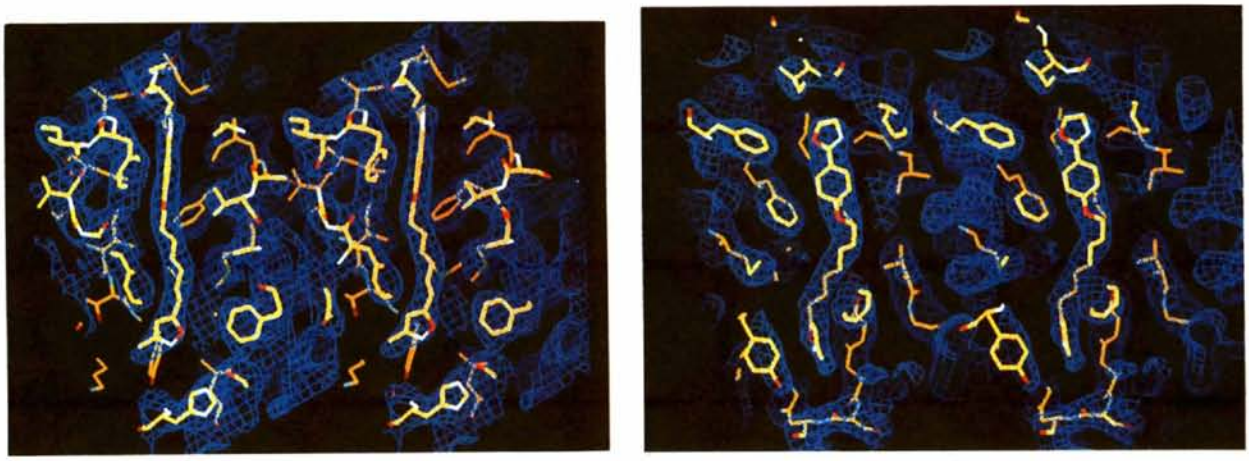

(a) (b)

Fig. 4. Stereoviews of the 'unbiased' electron-density map in the immediate vicinity of bound WIN51711 in the center of the VP1 β-barrel of P3/Sabin. This map was calculated by applying non-crystallographic symmetry constraints to drug-complex data after initiating phasing with a deliberately incomplete 'omit' atomic model as detailed in the text. For greater clarity, portions of the map and model at the front and back of these views have been truncated. (*a*) is a side view of the pocket, seen from a viewpoint similar to Fig. 5(*a*). (*b*) is a top view of the pocket, seen from a viewpoint similar to Fig. 5(*b*). Both (*a*) and (*b*) include a portion of the atomic model for the P3/Sabin complex with WIN51711.

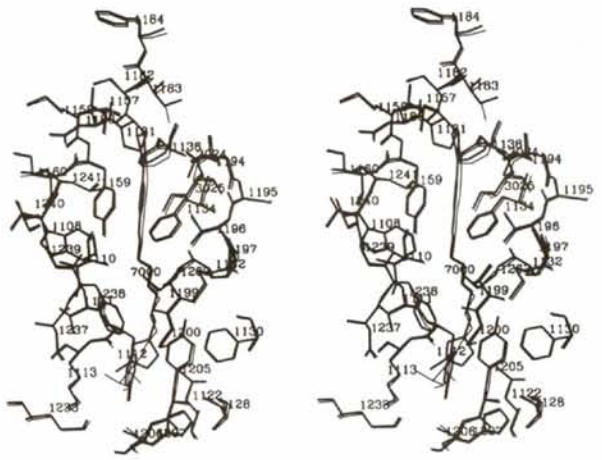

(a)

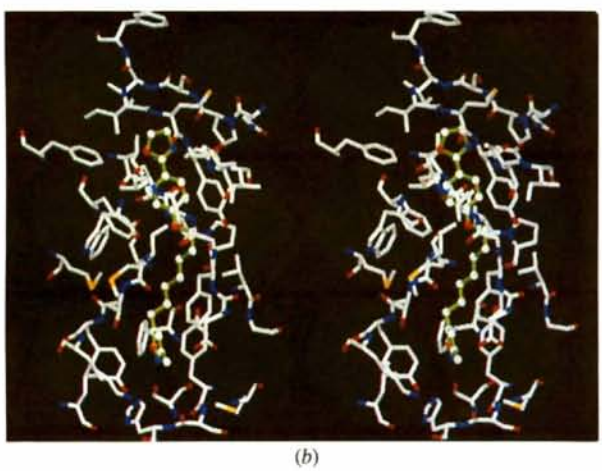

(b)

(c)

Fig. 5. Stereoviews of models of WIN51711 in complex with portions of the P3/Sabin structure. In all three panels, the drug is oriented vertically, with the buried hydrophobic end of the pocket closer to the top of the picture, and the polar more open end of the pocket closer to the bottom. (*a*) The atomic model for the drug complex (in thick lines) is shown superimposed on the native structure (in thin lines). In this side view of a portion of the protomer, residues within 7 Å of the bound drug or sphingosine are seen from the viewpoint of a neighboring fivefold-related protomer. The outer and inner surfaces of the capsid lie to the left and the right, respectively. As defined in the text, the pore connecting the pocket with the outer surface extends leftward in this picture from the isoxazole group of the drug, which is the ring seen face-on at the bottom end of the drug. Residue numbers are included as landmarks. (*b*) and (*c*) are both top views of the binding site, seen from identical viewpoints above the outer surface of the virion. (*b*) depicts a ball and stick model of the portion of the drug complex which lies within 7 Å of the bound WIN51711 molecule. Here, the isoxazole group of the drug is seen edge-on and the pore extends toward the viewer at the bottom of the picture. (*c*) is a ribbon representation of the main chain of the protomer, and is intended to put the close-up views in context. In this top view, β-strand *H* of the VP1 β-barrel can be seen crossing diagonally across the middle of the drug molecule.

ing drug complex in human rhinovirus 14 (HRV14). WIN51711 has been shown to be a more effective drug against polioviruses than it is in HRV14 (Pevear *et al.*, 1989; Grant *et al.*, 1994). The present study is the first time that it has been possible to assess the structural effects of binding the same broad-spectrum antipicornavirus agent both to poliovirus and to rhinovirus. This comparison should prove to be particularly valuable for the critical assessment of existing proposals for the mechanism of drug action. Moreover, the structure of the complex of WIN51711 with P3/Sabin provides a useful addition to the growing body of experimental information relevant to elucidating the physiological role(s) of the lipid-binding pocket in the life cycles of poliovirus and rhinovirus.

Materials and methods

Virus propagation and crystallization

P3/Sabin was prepared from a low-passage seed stock of a plaque isolate (P3/Leon/12a$_1$b plaque 411) obtained from Dr Philip Minor (NIBSC, London). The virus was propagated in HeLa cells, purified by differential centrifugation and CsCl density gradient fractionation as described elsewhere (Baltimore, Girard & Darnell, 1966). The purified virus was concentrated by pelleting and was resuspended at a concentration of approximately 10 mg ml^{-1} in 1 *M* NaCl in PMC7 buffer (10 m*M* PIPES, 5 m*M* $MgCl_2$, 1 m*M* $CaCl_2$, pH 7.0). The purified virus was crystallized by microdialysis *versus* progressively lower concentrations of NaCl in PMC7 buffer at 277 K. Crystals generally began to appear at approximately 0.6 *M* NaCl and crystal growth was complete in one to two months. As previously reported (Filman *et al.*, 1989), P3/Sabin crystallizes in the orthorhombic space group *I*222 with a = 321.1, b = 358.6 and c = 381.8 Å. The crystals contain 1/4 virus particle per asymmetric unit and thus express 15-fold non-crystallographic redundancy.

Preparation of drug–virus complexes

WIN51711 (disoxaril) was obtained from Mark McKinlay and Dan Pevear (Sterling-Winthrop). The solid drug was dissolved at a concentration of approximately 10 mg ml^{-1} in neat dimethyl sulfoxide and this stock solution was stored at 193 K until use. Fresh crystals grown in dialysis buttons were cleared of the virus in solution by washing with PMC7 buffer and subsequently equilibrated *versus* a synthetic mother liquor consisting of 25%(*v*/*v*) ethylene glycol in PMC7. Saturated solutions of disoxaril in the synthetic mother liquor were prepared by adding the stock solution until the mixture turned turbid, and clearing undissolved material by centrifugation for 10 min in an Eppendorf microcentrifuge. Crystals were transferred into the saturated drug solution, soaked for two weeks at 277 K, and mounted in sealed quartz capillary tubes for data collection.

Data collection and processing

Three-dimensional diffraction data were collected at 261 K using Cu $K\alpha$ radiation from an Enraf–Nonius GX-13 rotating-anode generator operated at 40 kV, 55 mA with a 100 μm focus and Franks mirror optics. 0.5° oscillation photographs were obtained from 3–4 h exposures. Photographs were digitized on a 50 μm raster using an Optronics PixelGetter film scanner controlled by a locally developed software interface (S. Crainic & D. J. Filman, unpublished work). Crystal orientation parameters for each photograph were estimated and refined by an autoindexing procedure (T. O. Yeates & D. J. Filman, unpublished work). Estimates for the intensities of the reflections on each photograph were obtained by applying a background-removal filter to the image and then deconvoluting the resulting filtered image. Here, the filtered image in each region is modeled as the convolution of a common filtered profile with a set of delta functions located at the predicted spot positions. (Grant, Filman, Fujinami, Icenogle & Hogle, 1992; D. J. Filman, unpublished work). Films were scaled and post-refined (by the method of Winkler, Schutt & Harrison, 1979), using the Fourier transform of the icosahedrally averaged native P3/Sabin electron-density map as the reference. The scaled data were merged to form the final three-dimensional data set.

Model/phase refinement

An initial symmetry-averaged drug-minus-native difference map was obtained using observed structure-factor magnitudes from the virus–drug complex, and phases from the native structure factors corresponding to the transform of the symmetry-constrained native P3/Sabin 'averaged F_o' map. Molecular replacement was initiated using a phasing model from which residues close to significant difference electron-density features had first been removed. These phases were then refined by a local implementation of the method of Bricogne (1974), alternately imposing non-crystallographic symmetry constraints on the map by averaging it, and amplitude constraints on the Fourier terms obtained by transformation of the averaged map.

Atomic models for the virus and the drug were built to fit icosahedrally constrained 'F_o' maps using the graphics program *FRODO* (Jones, 1978) modified to incorporate T = 1 icosahedral symmetry. Atomic models were optimized with respect to this map by a pseudo-real-space refinement procedure, minimizing a residual with a stereochemical and a crystallographic component. The gradient of the stereochemical component was provided by the *X-PLOR* program (Brünger, Kuriyan & Karplus, 1987). The crystallographic component and its gradient were evaluated over the volume of an arbitrary pseudo-

cell (the 'protomer box') which is sufficiently large to comfortably enclose a complete chemically continuous poliovirus protomer, together with whatever fragments of symmetry-related protomers happen to lie sufficiently close to the box to contribute to it. This refinement seeks to minimize the discrepancy between the 'phased' Fourier transforms of model-based electron density and authentic symmetry-constrained electron density, when each transform is calculated in the arbitrary protomer box volume, and scaled in a resolution-dependent fashion. The ability of this inexpensive strategy to duplicate the results of more conventional refinement methods has been confirmed (Jacobson *et al.*, 1995).

Further improvement of the phases and the atomic models was accomplished by periodically re-initiating the phase constraint procedure with the current partially refined atomic model. Phases derived from this model were used to reinitiate the refinement *versus* the non-crystallographic symmetry constraints, and iterative averaging was continued for about 20–25 cycles to convergence. This most recent icosahedrally constrained 'F_o' map then provided a new standard for the further rebuilding or refinement of the model.

Estimation of drug occupancy

Occupancy of the bound drug molecule was estimated by three methods described in detail by Grant *et al.* (1994). First, using the method of Smith *et al.* (1986), a series of occupancy-corrected electron-density maps was computed (for various values of k) from coefficients ($F_{drug,obsd} - kF_{native,obsd}$) and assessed for interpretability by visual inspection. Here, F_{native} and F_{drug} represent the resolution-bin-scaled Fourier transforms of protomer-box electron-density maps of the native and drug–complex structures, respectively. Second, a more quantitative assessment was obtained by comparing $F_{drug,obsd}$ with various linear combinations of the atomic model-based $F_{drug,calc}$ and $F_{native,calc}$ using the $R(1)$ statistic defined in Fig. 2. Third, an estimate of the total occupancy of bound ligand was obtained by refining the occupancies of individual drug atoms against $F_{drug,obsd}$, and assigning the average of these occupancies to the drug as a whole.

Results

Diffraction data

The three-dimensional data set was assembled from 14 oscillation photographs acquired from four crystals. A total of 256 545 reflection intensities were measured of which 149 190 were unique. These data were pruned further to remove those reflections which had been observed with a partiality less than 50%, and to eliminate a very small number (~0.6% of the total) which had been flagged as very poorly measured during the integration process. The final 2.9 Å data set consisted of 121 440 unique reflections with an R_{sym}* of 16.6% (14.6% for 47 214 fully recorded reflections). Although this data set is only 25% complete with respect to the crystallographic asymmetric unit (Fig. 2), 15-fold non-crystallographic symmetry results in the data set being generously oversampled with respect to the icosahedral asymmetric unit. The merging statistics for the data set are within the range normally observed for native poliovirus crystals. Neither the appearance of the films nor the merging statistics provided any indication that the introduction of the drug had resulted in any deterioration of the quality or resolution of the data.

Difference map

The merged data were used to calculate an icosahedrally averaged $F_{drug} - F_{native}$ difference map (Figs. 3*a* and 3*b*), which provides the most sensitive and objective possible assessment of the actual differences between the native and drug-bound structures. With the exception of four minor features on the outer surface of the virus which are explained below, all of the most significant positive and negative peaks in the difference map are located within the ligand-binding pocket. Only seven significant features can be seen in the lipid-binding region of the difference map. Three of the features are located at the deeply buried hydrophobic end of the pocket (seen at the top of the figure); four of the features are located near the exterior surface, at the polar end of the pocket (seen at the bottom of the figure); and none of the features is associated with the intervening region of the binding site. These three regions of the binding pocket will be shown to correspond to three distinct portions of the WIN51711 molecule. The strong features at the two ends of the pocket provide convincing evidence that the drug has substituted with high occupancy into the crystals during the period of the soak. The lack of difference density in the central region of the pocket suggests that the aliphatic linker of the WIN51711 molecule must occupy a conformation which is very similar to that of the central region of the normal substituent (modeled as sphingosine). The lack of significant difference density elsewhere in the structure (except in the known ion-binding sites, as noted below) suggests that the drug is able to bind with minimal local conformational adjustments of the viral capsid and without causing detectable long-range effects.

Structure determination

The structure of the drug–virus complex was solved by molecular replacement using the model of native P3/Sabin to derive preliminary phase estimates. In order to minimize possible phase bias, all solvent atoms as well as all atoms associated with significant difference density in the icosahedrally averaged difference maps were

* R_{sym} compares multiply measured individual corrected intensities (I_{hj}) with their σ-weighted mean $\langle I_h \rangle$. $R_{sym} = (\Sigma_h \Sigma_j |I_{hj} - \langle I_h \rangle|)/(\Sigma_h \Sigma_j \langle I_h \rangle)$.

removed from the phase calculations. The atoms omitted included the sphingosine molecule and main-chain and side-chain atoms for six amino-acid residues (Cys1086, Ile1183, His1207, Cys2174, Leu1294 and His3230).* The molecular-replacement phases were refined by the application of non-crystallographic symmetry constraints to the observed structure-factor magnitudes using the iterative procedure of Bricogne (1974). The final cycle of this refinement yielded an icosahedrally constrained 'unbiased' electron-density map (Figs. 4*a* and 4*b*). This map contained readily interpretable electron-density features for the drug and for surrounding protein side chains. The density provided unambiguous indications for both the orientation and the conformation of the drug molecule, and was consistent with the suggestion from the difference map that drug binding was accommodated without significant alteration of the local protein structure.

Overview of the binding site

For clarity, the residues of VP1 and VP3 which form the lipid-binding pocket in P3/Sabin are presented in only two orientations in this manuscript. The first orientation, corresponding to a view from the outer surface of the virus, is shown in Figs. 5(*b*) and 5(*c*). Fig. 5(*c*) places the bound drug molecule in the context of a complete protomer, which is shown as a ribbon representation of the main chain. Here, the binding site is being viewed from the outside of the virus, looking through the shorter flatter β-sheet (strands *C*, *H*, *E* and *F*) of the antiparallel β-barrel of capsid protein VP1. The

* The residue-numbering convention used throughout this manuscript uses a four-digit number where the first digit identifies the capsid protein (1 for VP1, 2 for VP2, 3 for VP3 and 4 for VP4) and the last three digits identify the residue number. For example, 1086 is residue 86 of VP1.

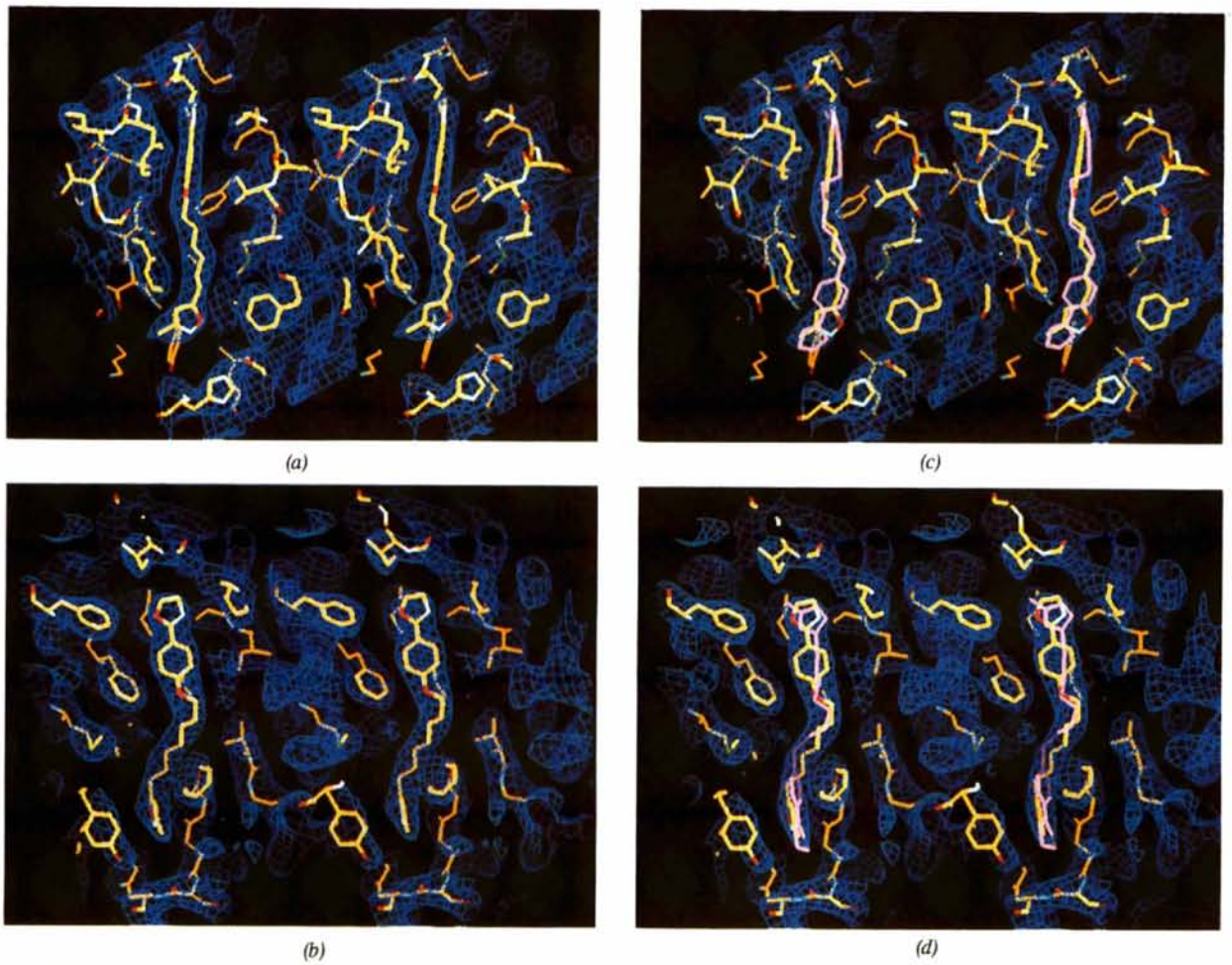

Fig. 6. The ability of 15-fold non-crystallographic symmetry constraints to minimize the effects of deliberate model bias in the P3/Sabin complex with WIN51711. As explained in the text, a substantially correct atomic model of the complex, with the isoxazole group of WIN51711 located in the outer pocket, was used to initiate phasing in the refinement that produced the electron-density maps shown in (*a*) and (*b*). An incorrect model of the drug, shown in pink, with its isoxazole group located at the buried end of the pocket, was used to initiate phase refinement for the maps in (*c*) and (*d*). For greater clarity, portions of the map and model at the front and back of these views have been truncated and portions of the atomic model further than 7 Å from the drug have been omitted. (*a*) and (*c*) are side views of the pocket, seen from viewpoints similar to Fig. 5 (*a*). (*b*) and (*d*) are top views, seen from viewpoints similar to Fig. 5(*b*).

drug molecule is oriented nearly vertically in the picture, and β-strand *H* runs diagonally in front of it, partially obscuring the phenoxy group of the drug in this view.

Fig. 5(*b*), in an identical orientation, shows a close-up view of the residues in the vicinity of the bound WIN51711 molecule which form the binding pocket in P3/Sabin. In this view, the drug extends from the top of the figure to the bottom and residues from the outer surface appear in the front. At the top of the picture, the most deeply buried portion of the drug is seen to be surrounded by a substantially hydrophobic environment. Portions of the ligand which are at the bottom of the picture lie closer to the outer surface of the virus, and interact with polar groups from the protein, and are exposed to the solvent. These interactions will be described in greater detail below. Note that a solvent channel can be seen near the bottom of the picture, extending directly forward from the isoxazole end of the drug molecule, towards the viewer. This channel, frequently referred to as a 'pore', connects the lipid-binding site with the outer surface at the bottom of the 'canyon'.

Fig. 5(*a*) shows the residues of the lipid-binding pocket in a second orientation, nearly orthogonal to that in Figs. 5(*b*) and 5(*c*). Here, the refined atomic model for native P3/Sabin, with its natural ligand modeled as sphingosine, is shown in thin lines; and the corresponding model for P3/Sabin with drug bound is drawn with thick lines. Residue numbers are included as landmarks so as to make the following description of the structure easier to understand. In this view from the 'side' of the protomer, the outer surface of the virus is located towards the left of the picture, and the inner surface of the capsid is located towards the right.

Figures in this manuscript which show the phenyloxazoline ring systems nearly edge-on in poliovirus (namely Figs. 3*a*, 4*a*, 5*a*, 6*a*, 6*c*, 7, 8 and 9) are all drawn from substantially similar vantage points along the 'side' of the protomer. Figures which show the isoxazole group nearly edge-on in poliovirus (namely Figs. 3*b*, 4*b*, 5*b*, 5*c*, 6*b*, 6*d* and 10) are all similar views from the outer surface.

The hydrophobic inner pocket

The shape of the electron-density feature for the bound ligand at the closed hydrophobic end of the pocket is entirely consistent with the presence of the phenyl and oxazoline rings. The density is flattened in one dimension (Fig. 4*a*), thus restricting the plane of these nearly coplanar rings to a unique orientation. The 'flip' of the oxazoline group (corresponding to an exchange of the N atom and the C atom of the five-membered heterocyclic ring) cannot be determined with confidence. However, the orientation has tentatively been assigned assuming that the slightly less electronegative N atom is more likely to occupy the position on the side of the ring which is in van der Waals contact with the carbonyl O atom of Pro1181.

The central region.

The electron density in the central region of the pocket provides a clear indication for the conformation of the aliphatic linker region of the drug molecule. Given the flexibility of this region of the molecule, the density is of surprisingly good quality, and a model for the ether O atom and C11–C17 was easily built with low-energy torsions. Consistent with the lack of difference electron density in this region of the averaged difference maps, the conformation of the aliphatic linker is very similar to that observed for the corresponding region of the sphingosine model in the native virus structure. As shown in Fig. 1 and Table 1, the chain is in a generally extended conformation (corresponding to a series of 180° dihedral angles) except for a single 'dog-legged' bend, corresponding to a 60° dihedral about the bond between C11 and C12. This bond lies at the end of the aliphatic chain, just adjacent to the phenoxy group of WIN51711.

The polar outer pocket

The electron density in the polar end of the pocket provides a clear indication for the preferred orientation of the isoxazole ring. Thus, the density is obviously thinner in one dimension (Fig. 4*b*), establishing the plane of the ring, and it is shaped somewhat like a boot (Fig. 4*a*), indicating the position of its methyl substituent. The indications for a single predominant orientation of the isoxazole ring is in sharp contrast to the relative disorder of the polar head group of sphingosine in the native structure (Filman *et al.*, 1989) and with the evidence for multiple conformations of the terminal benzoyl ester groups which occupy the

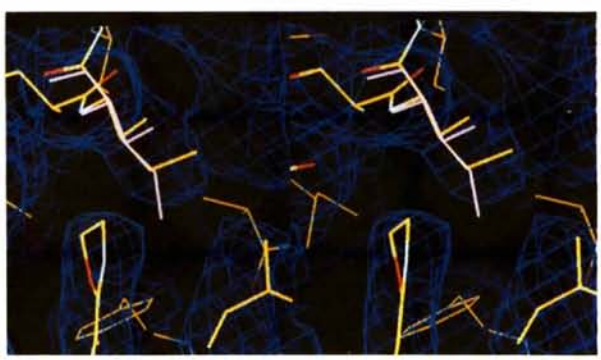

Fig. 7. Stereoview of the unbiased electron-density map in the vicinity of Ile1183 in the P3/Sabin complex with WIN51711. The calculation of this map is explained in the text. This is a side view, similar in viewpoint to Fig. 5(*a*). Electron density for the bound oxazoline group is visible at the bottom of the picture. The atomic coordinates shown in purple represent the conformation of Ile1183 in the structure of native P3/Sabin and the rest of the coordinates belong to the model of the drug–virus complex. Note that the native conformation of the Ile1183 side chain would be in steric conflict with the oxazoline ring.

corresponding position in poliovirus complexes with the drugs developed by Janssen (Grant *et al.*, 1994)

Confirmation of the orientation of the drug in the pocket

The clarity of the orientation of the drug in the pocket was surprising in light of the apparent ambiguity of the drug orientation in the previously reported complex in rhinovirus 14 (Smith *et al.*, 1986, Badger *et al.*, 1988). In order to confirm that the orientation had been correctly assigned we performed the following experiment. Models for the drug in the correct orientation (with the isoxazole ring near the pore) and in an incorrect orientation (with the isoxazole ring in the buried end of the pocket) were fitted to the density, and used as the starting point for two independent phase refinements *versus* the non-crystallographic symmetry constraints. After both refinements had converged, the two averaged maps were compared (Fig. 6). The two maps are remarkably similar; and both maps provide a clear indication that the orientation of the ligand with the isoxazole ring close to the pore is correct.

Lack of structural changes associated with drug binding

The P3/Sabin complex with WIN51711 is remarkable for the limited extent of the structural changes induced by drug binding. Indeed, of the six difference-density peaks in the protein region of the initial difference-density maps, four appear to be trivial and totally unrelated to drug binding. These include difference-density peaks in the vicinity of Cys1086, Cys2174, Leu1294 and His3230. All four residues are located in highly exposed positions on the outer surface of the virus, fairly distant from the pocket. The difference density in the vicinity of His3230 is attributable to a difference in the occupancy of a previously described cation-binding site (possibly Zn^{2+}). This site is poorly occupied in the native virus structure because of the inclusion of EDTA at late stages of the preparation of the virus used to solve the native structures and more highly occupied in more recent structures from this laboratory because of the omission of EDTA from more recent virus-purification protocols. The density maps show obvious indications both for the bound cation and for a shift of the imidazole group of His3230 toward the cation site. The maps also indicate a shift in the same direction of the side chain of Leu1294 which is located immediately adjacent to His3230. The difference-density features in the vicinities of Cys2174 and Cys1086 are both positive peaks, rather than the paired positive and negative features which would suggest changes in the positions of the sulfhydryl side chains. These differences might, therefore, be attributable to low levels of oxidation or other chemical modification of these surface residues during the preparation of the drug–virus complexes.

All of the remaining large difference-density features associated with protein are located in the immediate vicinity of the bound drug and are associated with the side chains of Ile1183 and His1207. These difference-density features appear to arise from small but significant shifts in the side chains in response to drug binding in the pocket. Although the shifts are small, they warrant attention, if for no other reason than that they are the largest shifts which occur in the viral proteins on drug binding. These two side-chain adjustments are described in more detail below.

*The movement of Ile*1183

In the innermost portion of the ligand-binding site, closely associated with the bulky head group of the bound drug, the difference map (Fig. 3) contains a pair of difference electron-density peaks, one positive and one negative, located on either side of the side chain of Ile1183 (located near the top of Figs. 3*a* and 3*b*). This pair indicates that drug binding has caused a change in the conformation of the isoleucine side chain. The negative peak roughly corresponds to the location of CD1 in P3/Sabin with its less bulky natural ligand bound and the positive peak corresponds to the location of this atom in the complex with WIN51711. This interpretation is confirmed by the appearance of the icosahedrally constrained 'omit' electron-density map (Fig. 7) which shows the conformation of the side chain unambiguously. Presumably, the reorientation of the side chain (corresponding to a 2.3 Å movement of CD1) is necessary to avoid steric conflicts with the bulkier drug molecule. Close inspection of the density indicates that in each of the native and drug-bound states, the isoleucine side chain can be model built convincingly in one of its low-energy (*i.e.* staggered) conformations. This confirms the interpretation of the difference electron-density features, as it is consistent with the expectation that the conformation of aliphatic side chains should principally be governed by van der Waals forces.

*The movement of His*1207

A pair of difference electron-density peaks (Fig. 3*a*), one positive and one negative can be seen to the right and the left of the imidazole group of the side chain of His1207, respectively. These peaks confirm that the imidazole group is situated further to the right in P3/Sabin when WIN51711 is bound. Contrary to what one might expect, however, the shift does not appear to be caused by steric conflicts between the imidazole and isoxazole groups, despite the apparent increase in the bulk of this portion of the ligand, relative to native, and the apparent extension of the isoxazole ring further to the right in the pocket. Instead, measurements taken from the refined atomic models suggest that His1207 (which is conserved among poliovirus sequences, Table 2) provides a favorable van der Waals contact for the sphingosine molecule (with O3 of sphingosine some 3.70 Å from ND1 or CD2

Table 2. *Sequence conservation among the structurally conserved amino-acid residues lining the hydrophobic pocket at the center of the VP1 β-barrel in polio- and rhinoviruses*

Three representative strains are shown for each virus. Residue numbers are provided in terms of the P3/Sabin (upper) and HRV14 (lower) sequences. Each listed residue includes at least one atom within 5.0 Å of the bound drug molecule.

Poliovirus	1110	1112	—	1128	1130	1132	1134	1136	1157	1158	1159	1181
P2/Lansing	Ile	Tyr	—	Ser	Phe	Met	Phe	Phe	Ile	Met	Tyr	Pro
P1/Mahoney	Ile	Tyr	—	Ser	Phe	Met	Leu	Phe	Ile	Met	Tyr	Pro
P3/Sabin	Ile	Tyr	—	Ser	Phe	Met	Phe	Phe	Ile	Met	Tyr	Pro
Rhinovirus	1104	1106	1116	1122	1124	1126	1128	1130	1150	1151	1152	1174
HRV14	Ile	Leu	Leu	Val	Phe	Ser	Tyr	Ile	Ala	Met	Tyr	Pro
HRV16	Ile	Leu	Phe	Ala	Phe	Ser	Ile	Met	Tyr	Met	Tyr	Ala
HRV1A	Ile	Leu	Phe	Val	Phe	Ser	Ile	Leu	Tyr	Met	Tyr	Met
Poliovirus	1182	1183	1194	1196	1199	1205	1206	1207	1238	1241	3024	3025
P2/Lansing	Ser	Val	Ile	Val	Val	Tyr	Ser	His	Phe	Leu	Ala	Ile
P1/Mahoney	Ser	Ile	Ile	Val	Val	Tyr	Ser	His	Phe	Leu	Ala	Leu
P3/Sabin	Ser	Ile	Ile	Val	Val	Tyr	Ser	His	Phe	Leu	Ala	Ile
Rhinovirus	1175	1176	1186	1188	1191	1197	1198	1199	1221	1224	3024	3025
HRV14	Ser	Val	Phe	Val	Val	Tyr	Asn	Cys	Met	Met	Ala	Leu
HRV16	Ser	Val	Phe	Leu	Leu	Tyr	Tyr	Met	Met	Leu	Ala	Leu
HRV1A	Ser	Ile	Phe	Ile	Leu	Tyr	Tyr	Met	Met	Ile	Ala	Leu

of the histidine) whereas His1207 gets no closer to the drug molecule than 4.25 Å, relative to N20.

The interaction of WIN51711 with His1207, while not a specific charge interaction, is reminiscent of the binding of palmitate (see Fig. 1) by the chimeric poliovirus V510 (Yeates *et al.*, 1991). Thus, rather than bending slightly leftward and forward toward the pore (Fig. 5*a*), as the longer sphingosine molecule does, the polar head-group of palmitate (like WIN51711) turns slightly rightward and downward to interact with the imidazole group of His1207. Here, the ability of the ligand to fit in the portion of the lower pocket to the far right might conceivably be as much a matter of the size of the ligand as its charge distribution.

Badger, Krishnaswamy *et al.* (1989) have reported that many of the observed drug-resistant mutants of HRV14 involve replacement of Cys1199, at the structurally analogous site, with bulkier residues such as Tyr and Trp, which presumably interfere sterically with drug binding. In poliovirus, however, none of the drug-resistant mutants observed thus far have contained mutations in this site (Mosser, Sgro & Rueckert, 1995), perhaps because poliovirus mutants which are sterically blocked from binding their native ligands are unlikely to be viable.

Similarity with native structure

The remarkable similarity of the P3/Sabin–WIN51711 complex to the structure of the native virus contrasts dramatically with the large structural changes observed upon drug binding to HRV14. This striking difference in the extent of structural rearrangement is largely attributable to the presence of a ligand in the native P3/Sabin structure and the absence of a ligand in native HRV14. It should be noted, however, that the structural changes required to accommodate WIN51711 in P3/Sabin are even smaller than the minor changes associated with the binding of several antiviral compounds from Janssen to P3/Sabin (Grant *et al.*, 1994). This might be due to the greater degree of flexibility provided by the longer aliphatic linker of WIN51711, and to the similarity of this portion of the drug to the part of the natural ligand which occupies this site in the virion.

Model/phase refinement

An atomic model of the virus adjusted for the minor changes in the capsid protein, and containing the bound WIN51711 molecule in its correct orientation, was used to initiate a new round of phase refinement *versus* the non-crystallographic symmetry constraints. The model and the phases were further refined by alternating cycles of manual rebuilding, automated refinement of the atom positions using the novel refinement protocol described in the *Methods* section, and the application of non-crystallographic symmetry constraints. After convergence of the final round of phase refinement, the non-crystallographic R factor and correlation coefficient for all data from 30 to 2.9 Å were 20.13% and 0.9213, respectively. A resolution breakdown of the statistics of the phase refinement is provided in Fig. 2.

The final refined model included 6631 non-H atoms of the protein, 25 atoms of WIN51711 and restrained individual isotropic temperature factors. To assign an occupancy factor to the bound drug molecule, all three occupancy tests described in the *Methods* section were carried out (using an identically refined model of native P3/Sabin for tests where such a model was required.) Using these methods, it was estimated that sphingosine had been replaced by drug in approximately 100% of the binding sites of the crystal. Statistics indicating the agreement of the final model with stereochemical standards are provided in Table 3. A resolution breakdown of the model-dependent R factor which is based on the final model is included in Fig. 2.

Table 3. *Statistics for the refined model*

$R(1)_{cryst}$ is the model-based crystallographic R factor, as defined in Fig. 2. The other statistics represent root-mean-square (r.m.s.) deviations of the atomic coordinates from idealized stereochemical standards. Because of the interest in establishing the significance of small differences between the native and WIN51711 poliovirus structures, the geometric constraints were held significantly tighter than is normal for structures at 2.9 Å resolution. This, together with the incompleteness of the data and the lack of a solvent model for the current model for the drug complex, results in the relatively high crystallographic residual shown here. Other drug complexes have comparable values of R_{cryst} (Grant *et al.*, 1994), while refined native structures with similar constraints, but based on complete data and including solvent models, have crystallographic residuals in the high teens or low twenties (Jacobson, Hogle & Filman, 1995).

$R(1)_{cryst}$	0.316
Bond lengths (r.m.s.) (Å)	0.012
Bond angles (r.m.s.) (°)	2.6
Variable torsion angles (r.m.s.) (°)	25.8
Fixed dihedrals angles (r.m.s.) (°)	1.1

Discussion

Overall comparison of the native structures of poliovirus and rhinovirus capsid proteins

The native structures of P3/Sabin and HRV14 are very similar to one another. Both contain three major capsid proteins, VP1, VP2 and VP3, and a small internal capsid protein, VP4. Each of the major proteins consists of an eight-stranded antiparallel β-barrel (whose β-strands are conventionally labeled *B–I*). Strands of the β-barrels are connected by loops, many of which are located on the exterior surface of the virus (and which are named after the β-strands they connect). Poliovirus and rhinovirus have very similar main-chain structures, except in a small number of the connecting loops, and in the conformation or degree of order in portions of VP4 and the amino and carboxyl extensions of the major capsid proteins (Table 4). Except as listed in Table 4, the remaining 686 residues of P3/Sabin and HRV14 can be regarded as structurally equivalent. For these equivalent residues, the r.m.s. positional difference between corresponding Cα atoms in the atomic models is only 0.6 Å.*

Comparison of the drug-binding sites in P3/Sabin and HRV14

In the following sections, the structures of the native and drug-bound HRV14 are compared with the structure of P3/Sabin. As indicated in the preceding section, drug-bound P3/Sabin is remarkably similar to P3/Sabin with its naturally occurring ligand bound. In fact, all of the significant differences involve alterations in side-chain conformation. Thus, the main-chain structures of native and drug-bound P3/Sabin are nearly indistinguishable from one another. Comparisons below of HRV14 with the structure of drug-bound P3/Sabin, therefore, also are equally valid for the native poliovirus structure.

Table 4. *Significant differences between the main-chain structures of P3/Sabin and HRV14*

Capsid protein	Location	P3/Sabin residues	HRV14 residues
VP1	Amino extension	1024–1030	1017–1019
	Amino extension	1067–1071	1057–1061
	BC loop	1098–1101	1088–1095
	DE loop	1141–1151	1135–1144
	FG loop	1186–1191	1179–1183
	GH loop	1214–1228	1206–1211
	Carboxyl extension	1232–1240	1215–1223
	Carboxyl extension	1289-1291	1273-1276
	Carboxyl extension	1297	1283–1285
VP2	*EF* loop	2135–2140	2135–2140
	EF loop	2155–2170	2155–2162
	EF loop	2174–2176	2166–2168
	HI loop	2238–2243	2230–2235
	Carboxyl terminus	2267–2271	2259–2262
VP3	*B* strand interruption	3049–3062	3059–3061
	BC loop	3073–3081	3072-3079
	EF loop	3139–3141	3136–3138
	HI loop	3200–3201	3197–3198
	HI loop	3204–3207	3201–3204
	Carboxyl extension	3235	3232
	Carboxyl terminus	Disordered	3233–3236
VP4	Amino terminus	4001–4017	Disordered
	β strand	4023–4029	Disordered
	Middle	4042–4049	4041–4048

The solution of the crystal structure of WIN51711 in complex with P3/Sabin (here) and with HRV14 (Smith *et al.*, 1986; Badger *et al.*, 1988) provides the opportunity to determine how differences in the structure of the binding pocket are related to differences in the mode of drug binding and how these, in turn, can be used to account for differences in the ability of drugs of this kind to inhibit viral growth. A specific issue to be addressed is the finding that WIN51711 is a 15-fold (Andries, personal communication; Grant *et al.*, 1994) to 19-fold (Pevear *et al.*, 1989) better inhibitor of P3/Sabin than it is of HRV14. Superimposed stereoviews of the drug-binding sites of P3/Sabin and HRV14, each occupied by WIN51711, are shown in Fig. 8. The P3/Sabin complex, drawn in thick lines, was determined in the present study. The atomic model for the HRV14 complex, shown in thin lines, was obtained from the Protein Data Bank file 2R04 (PDB, Bernstein *et al.*, 1977). The atomic models were superimposed simply by referring them both to the same icosahedral frame of reference. Structurally analogous residues which participate in binding WIN51711 in the P3/Sabin or HRV14 complexes are listed in Table 5 for reference.

Comparison of the inner pocket

The inner aromatic region of the drug-binding site appears near the top of Fig. 8. In this area, P3/Sabin and HRV14 have nearly identical main-chain conformations, and substantially similar amino-acid side chains in remarkably well conserved positions and orientations. The sequence identities (see Tables 2 and 5) include Ile1110

* Atomic coordinates have been deposited with the Protein Data Bank, Brookhaven National Laboratory (Reference: 1PIV). Free copies may be obtained through The Managing Editor, International Union of Crystallography, 5 Abbey Square, Chester CH1 2HU, England (Reference: GR0502) or from the authors upon request.

Table 5. *Structural alignment between residues of P3/Sabin and HRV*14 *which form the lipid-binding pocket*

For each virus, amino-acid residues having any atom within 5 Å of the bound drug are included, and aligned with structurally equivalent residues from the other viruses. Residues making specific contacts, 4.0 Å or less, with the bound WIN51711 molecule are indicated by naming the portion of the drug molecule involved in the contact.

Drug region	Protein region					Drug region
	P3/Sabin			HRV14		
	1110	Ile	*CD* loop	Ile	1104	Aliphatic, phenyl
Isoxazole	1112	Tyr	*CD* loop	Leu	1106	
	—	—	*CD* loop	Leu	1116	
	1128	Ser	*D* strand	Val	1122	
	1130	Phe	*D* strand	Phe	1124	
	1132	Met	*D* strand	Ser	1126	
Phenyl	1134	Phe	*D* strand	Tyr	1128	Aliphatic
	1136	Phe	*D* strand	Ile	1130	
Oxazoline	1157	Ile	*E* strand	Ala	1150	
	1158	Met	*E* strand	Met	1151	
Phenyl	1159	Tyr	*E* strand	Tyr	1152	Phenyl
Oxazoline	1181	Pro	*F* strand	Pro	1174	
	1182	Ser	*F* strand	Ser	1175	
Oxazoline	1183	Ile	*F* strand	Val	1176	
	1194	Ile	*G*1 strand	Phe	1186	Oxazoline, phenyl
	1196	Val	*G*1 strand	Val	1188	
	1199	Val	*G*1 strand	Val	1191	
Isoxazole	1205	Tyr	*G*2 strand	Tyr	1197	Aliphatic
	1206	Ser	*G*2 strand	Asn	1198	Phenyl
	1207	His	*GH* loop	Cys	1199	Isoxazole
	—	—	*GH* loop	Asn	1219	Isoxazole
Aliphatic, isoxazole	1238	Phe	*GH* loop	Met	1221	Aliphatic
Phenyl	1241	Leu	*H* strand	Met	1224	Oxazoline
	3024	Ala	N-terminus	Ala	3024	Oxazoline
	3025	Ile	N-terminus	Leu	3025	Isoxazole
				HOH	8503	Isoxazole

(1104 in HRV14), Pro1181 (1174), Tyr1159 (1152), Val1196 (1188) and Ala3024 (3024). Highly conservative substitutions include Phe1134 (Tyr1128), Ile1183 (Val1176), Leu1241 (Met1224) and Ile3025 (Leu3025). The remaining substitutions, which are less conservative but preserve the hydrophobic character of the site, are Phe1136 (Ile1130), Ile1157 (Ala1150) and Ile1194 (Phe1186). As Fig. 8 shows, the two-ring system of WIN51711 occupies substantially the same position in HRV14 as it does in P3/Sabin except that it is inserted slightly less deeply into the pocket and that the plane of the rings have been rotated by, perhaps, 40°. This difference may be primarily due to the presence in HRV14 of a bulky phenylalanine side chain (Phe1186) in the position homologous to that of Ile1194 in P3/Sabin. (These side chains are located immediately to the right of the oxazoline group in Fig. 8.) Because the orientation of this Phe side chain appears to be constrained by the residues surrounding it, there does not appear to be any way to avoid a steric conflict with the oxazoline group of WIN51711, except by reorienting the oxyphenyloxazoline group.

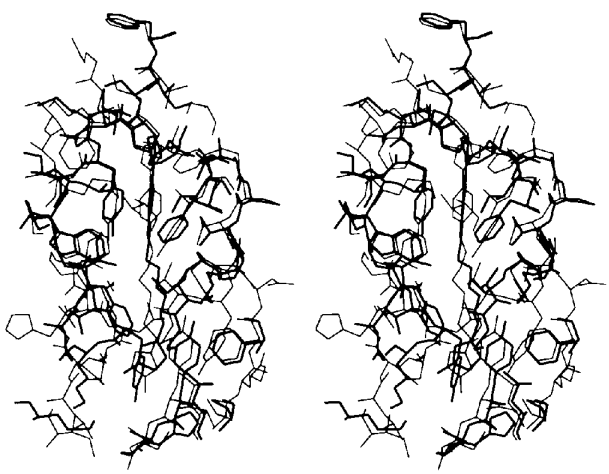

Fig. 8. Comparison of the structures of P3/Sabin and HRV14 in the immediate vicinity of the bound WIN51711 molecule. In this stereoview, superimposed atomic models of the P3/Sabin and HRV14 complexes are drawn in thick and thin lines, respectively. Residues further than 7 Å from the drug are omitted for clarity. This side view of the pocket is similar to that shown in Fig. 5(*a*).

While drug-bound P3/Sabin and HRV14 are very similar in the inner pocket, both differ noticeably from native HRV14 in the conformation of Tyr1152 (1159 in polio). In both drug-bound viruses, the side chains of Tyr1152 and Val1188 (1196) are located across the pocket from one another, some 7 Å apart, and provide hydrophobic contacts for both surfaces of the phenoxy group of the drug. In contrast, in native HRV14, a significant movement of the Tyr1152 side chain coupled with a smaller associated movement of the main chain (at the amino end of the *EF* loop) places the Tyr and Val less than 5 Å apart, which represents a significant constriction of the binding site. The proximity of these two side chains is, of course, inconsistent with the presence of a ligand though it represents the only major alteration in the structure of the inner pocket. Hence, once drug has been bound, the inner portion of the drug-binding site is remarkably similar in poliovirus and rhinovirus: the

drug orientation is similar, the structural conservation is striking and the degree of sequence conservation is impressive. This provides strong evidence that the biological role of the ligand-binding site in poliovirus is important in rhinoviruses, even though the site happens to be vacant in the native HRV14 crystal structure (Rossmann *et al.*, 1985).

Comparison of the middle pocket

In contrast with the structural conservation of the deepest portion of the drug-binding pocket, the binding site for the aliphatic linker in HRV14 is markedly different from that of poliovirus in two important respects. First, it is broader, and thus less restrictive, and secondly it is more polar. As it can be seen in Fig. 8, below and to the left of the aliphatic linker, a bulky Phe side chain in P3/Sabin (1238) has been replaced by a more flexible methionine (1221) and the conserved Ile1110 (1104) has moved significantly leftward. Above and to the right of the chain, two hydrophobic residues, Met1262 and Met1132 in P3/Sabin, have been replaced by polar ones (His1245 and Ser1126 in HRV14), and the presence of serine has induced the binding of a fixed solvent molecule, apparently hydrogen bonded to the side chains of Ser1126 and Tyr1197. As a result of the broadening of the middle section of the pocket, and the increased polar character of its lower and right surfaces, the aliphatic linker of WIN51711 is displaced noticeably toward the left of Fig. 8. This moves the chain away from the polar residues on the right side of the pocket and towards the hydrophobic left side.

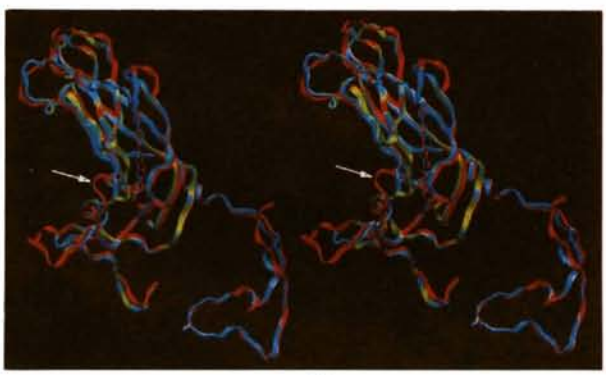

(*a*)

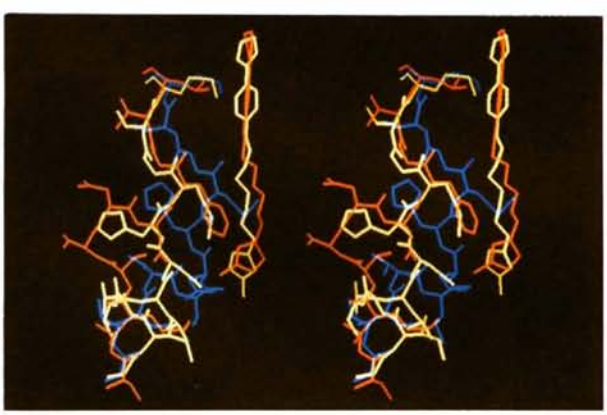

(*b*)

Fig. 9. Structural differences in the main-chain conformations of P3/Sabin and HRV14 that are associated with the binding of WIN51711. These stereo pairs are both side views, similar in viewpoint to Fig. 5(*a*). (*a*) Superimposed ribbon representations of the main-chain tracing of capsid protein VP1. Native HRV14 is yellow, drug-bound HRV14 is blue and drug-bound P3/Sabin is red. (*b*) Superimposed detailed models of the carboxyl end of the *GH* loop of VP1. Native HRV14 is blue, drug-bound HRV14 is yellow, and drug-bound P3/Sabin is orange. Residue numbers for the protein are listed in the text. In both (*a*) and (*b*) WIN51711 from the two drug-bound structures is shown.

Without a restrictive binding site, such as that in P3/Sabin, and with the pocket partially polar in character, the aliphatic chain of WIN51711 could be expected to show considerable flexibility in the HRV14 complex, and thus significantly less order in the crystal structure. Consistent with this, the atomic model for WIN51711 in HRV14 appears to have been constructed with several high-energy torsions in the linker region (specifically 140, 101, 96, 120 and 127°, in that order, see Fig. 1, Table 1). This suggests both that model building was difficult in this region, and that multiple conformations are likely to be present in the actual rhinovirus complex. In view of the marked conformational similarity between sphingosine and WIN51711 in P3/Sabin, and the large number of hydrophobic side chains available in this area, the site seems entirely suitable for the binding of an aliphatic chain. In contrast, the corresponding portion of the pocket in HRV14 is clearly less well suited for binding the aliphatic chain because the channel is both too wide and too polar. This may account in part for the 15-fold lower efficacy of WIN51711 in HRV14 as compared with P3/Sabin.

Comparison involving the outer pocket and the carboxyl end of the GH loop

Differences between P3/Sabin and drug-bound and native HRV14 in the vicinity of the outer pocket are dominated by profound differences in the structure of a single region of the polypeptide chain. Specifically, residues 1231–1241 of poliovirus (corresponding to 1214–1224 of HRV14) form a connection between the carboxyl end of the *GH* loop of VP1 and the amino end of β-strand *H*. The three structures differ markedly in the conformation of these residues, but have much greater similarity outside of this region. Fig. 9 shows a superposition of these residues in the three structures. In native HRV14 the side chain of Met1221, and the peptide O atoms of 1221 and Asn1219 would be in steric conflict with the aliphatic chain of the drug. As shown in Fig. 9(*b*), significant rearrangement of the entire 11-residue chain repositions this methionine side group into a location and orientation analogous to that of Phe1238 in poliovirus. Both side chains form similar hydrophobic surfaces

extending parallel to the aliphatic portion of the drug. (In the case of HRV14, this is a wall of the middle pocket lying opposite the partially polar surface which is specific to rhinovirus.) As a result of this drug-induced rearrangement, the main-chain conformation of drug-bound HRV14 becomes very similar to that of poliovirus in residues 1231–1232 (1214–1215 in HRV14), and in residues 1238–1241 (1221–1224).

In contrast, the five intervening residues (1233–1237 in P3/Sabin, 1216–1220 in HRV14) are clearly very different in all three structures. These residues participate in forming the outer portion of the pocket and the solvent channel of the pore in P3/Sabin. In particular, these residues participate in forming the interface between symmetry-related protomers in P3/Sabin, but they are positioned away from the interface and obstruct the pore in both native and drug-bound HRV14. The relative obstruction in drug bound HRV14 is apparent in Figs. 10(*a*) and 10(*b*), which depict van der Waals surfaces for the poliovirus and rhinovirus atomic models, respectively, in the vicinity of the pore. In poliovirus the isoxazole group of WIN51711 is clearly visible from outside of the virus and is exposed to solvent. On the other hand, the bound drug molecule in HRV14 is barely visible and is inaccessible to solvent. This enclosure of the outer pocket in rhinovirus might suggest that binding of the isoxazole group involves more extensive interactions than in poliovirus and thus this group is more important in rhinovirus for the stabilizing effect of the drug.

The isoxazole group is similarly positioned in HRV14 and P3/Sabin, but oriented differently (see Fig. 8). Both the planes of the isoxazole rings and the substituent methyl groups are pointed in different directions in the two complexes. This difference can be accounted for by noting that the preferred orientation in HRV14, which is favored by a specific hydrogen-bonding pattern, would be precluded in P3/Sabin by steric conflicts. The outer pocket of HRV14 contains two potential hydrogen-bonding groups which are available for making charge–charge or hydrogen-bonding interactions. The first such group is a fixed solvent molecule which is positioned, in turn, by a network of hydrogen bonds involving the peptide N atoms of Leu1106 and Ser1107 and the side-chain O atom of Ser1107, all of which are located just beyond the carboxyl end of β-strand *C* of VP1. In the model of the WIN51711 complex with HRV14 (PDB2R04), the ring N atom of the isoxazole group is hydrogen bonded to this fixed water. The second potential hydrogen-bonding group projecting into the pocket is the side chain of Asn1219. Although this group does not appear to be involved in the binding of WIN51711 to HRV14, it was identified by Kim *et al.* (1993) as a specific contact for WIN54954 and might be involved in the binding of other drugs in this portion of the binding site. The corresponding residue in P3/Sabin, Asp1236, is unavailable for binding antiviral compounds, as it occupies a position distant from the bound drug. This residue is one of the five residues at the carboxyl end of the *GH* loop which differ significantly between P3/Sabin and drug-bound HRV14.

The second major cause of the differences in isoxazole binding is a steric effect shown in Fig. 8. In HRV14, one of the residues responsible for binding the fixed solvent, Leu1106, has its side chain rotated away from the viewer, towards the back of the picture. This side-chain position is, of course, consistent with the isoxazole orientation in HRV14. In contrast, the analogous side chain in P3/Sabin is Tyr1112, which is rotated toward the front of the figure, in a position inconsistent with the HRV14 conformation of the drug. These virus-specific structural differences, corresponding to some of

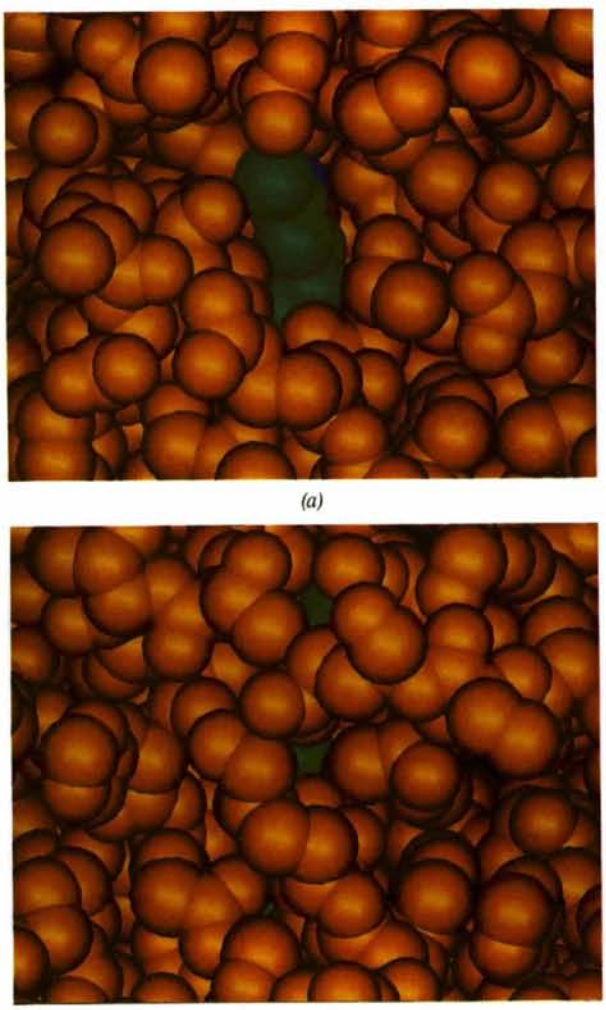

(a)

(b)

Fig. 10. Differences in the accessibility of WIN51711 when bound to P3/Sabin and HRV14. The outer surface of the capsid in the immediate vicinity of the pore is depicted as a van der Waals surface representation based on the atomic model of (*a*) drug-bound P3/Sabin and (*b*) drug-bound HRV14. Both (*a*) and (*b*) are top views, similar in viewpoint to Fig. 5(*b*). Note that the isoxazole group of the drug (shown in green) is more exposed in P3/Sabin, but inaccessible to solvent in HRV14.

the differences in interatomic contacts listed in Table 5, may represent an important cause of the virus-specific differences in drug efficacy.

Possible link between the GH and EF loops of VP1

In all of the structures there is a close interaction of the carboxyl end of the *GH* loop of VP1 with several residues at the amino end of the *EF* loop of VP1. When the structures of drug-bound and native HRV14 were compared, large drug-induced movements of Tyr1152 at the amino end of the *EF* loop and in the *GH* loop of VP1 widened the neighboring region of the inner pocket and allowed the accommodation of the phenoxy-oxazoline rings. These large movements appear to be coupled with a much smaller but still noticeable concerted shift of the *EF* loop away from the lipid-binding pocket and toward the adjacent fivefold-related protomer. This interface previously has been implicated in poliovirus as the site of specific mutations that affect temperature sensitivity of P3/Sabin (Macadam *et al.*, 1991; Filman *et al.*, 1989). The amino-acid sequence of this portion of the *EF* loop (residues 1161–1165 in P3/Sabin) is both striking (Pro-Pro-Gly-Ala-Pro) and conserved among polioviruses and rhinoviruses. We previously have argued that interactions involving this loop may play a role in drug binding and release (Grant *et al.*, 1994) and in regulation of conformational changes associated with thermal inactivation and cell entry (Filman *et al.*, 1989; Flore *et al.*, 1990; Grant *et al.*, 1994).

Basis of drug specificity and mechanism of drug action

WIN51711 is one of a large number of compounds which have been shown to inhibit the replication of poliovirus and human rhinoviruses by binding to the hydrophobic core of capsid protein VP1 and preventing the conformational changes in the capsid required for uncoating of the virus. Structural studies of antiviral drugs bound to poliovirus and rhinovirus have been undertaken, in part, to determine the structural basis of the specificity and strength of virus–drug interactions. Andries *et al.* have investigated the binding of a number of the existing antiviral drugs to a number of rhino-, polio- and coxsackieviruses and have shown that the viruses segregated into two groups (Andries *et al.*, 1990). One group of viruses, of which polioviruses and HRV14 are examples, are most effectively neutralized by longer drugs. The other group of viruses, exemplified by rhinoviruses 16 and 1A, are most effectively neutralized by much shorter drug molecules. One important objective of solving the structures of a variety of virus–drug complexes is to try to elucidate what properties P3/Sabin and HRV14 might have in common that differ from the properties shared by rhinoviruses 16 and 1A.

Comparison of the drug-bound structures of P3/Sabin and HRV14 provides a convincing structural explanation for the ability of both viruses to bind the same class of antiviral compounds. Thus, the high degree of structural conservation of the inner pocket is consistent with the observation that both viruses bind bulky aromatic ring systems in this site. Furthermore, studies of the binding of WIN compounds to HRV14 have indicated that bulkier, more highly substituted groups that fill the inner pocket more fully tend to be more effective antiviral compounds than less highly substituted ones (Kim *et al.*, 1993). This correlation is supported by observations in poliovirus that the relatively bulky Janssen and WIN compounds are able to displace the thinner natural ligand, and that the resulting complex is more stable than the native structure with 'pocket factor' bound.

The bulk of the substituent, however, cannot be the sole determining factor of antiviral activity. As reported in Grant *et al.* (1994), Andries has shown that Janssen compounds with very short aliphatic chains require anomalously large concentrations of drug to be effective against P3/Sabin, and structural studies by our laboratory have shown that these compounds differ from more effective ones by failing to fill the inner pocket completely. This emphasizes the importance of a sufficiently long 'tether' in permitting the bulky substituents to assume the correct positions and orientations in the inner and outer pockets.

Naturally, the inappropriate placement of bulky substituent groups on the drug molecule at positions which would conflict with the protein would prevent a ring system from occupying the inner pocket at all. Thus, in the binding of WIN51711 to HRV14 (Smith *et al.*, 1986), the addition of one or more methyl substituents to the oxazoline ring was sufficient to prevent the phenoxyoxazoline group from occupying the deepest portion of the pocket (though the methylated compounds were still capable of binding to the virus with their smaller ends most deeply buried).

In previous studies of the binding of antiviral compounds to rhinoviruses 16 and 1A (Oliveira *et al.*, 1993; Kim *et al.*, 1993) it has been suggested that the decreased affinity of these viruses for longer drugs (*i.e.* those with roughly seven-carbon linkers) and increased affinity for shorter drugs (those with five-carbon linkers) was primarily as a result of a foreshortening of the inner pocket, largely due to the presence of a bulky methionine side chain (1169 in the HRV1A sequence). This alteration in the shape of the inner pocket was reflected by a convincing difference in the path of the drug through the inner pocket, when the short-drug viruses were compared with HRV14. Hence, the results of the present study, indicating that the path of the drug in HRV14 strongly resembles that in poliovirus, confirms that this property does appear to be common to the known long-drug virus structures.

The importance of conformational changes in the virus for drug activity

At the time that the crystal structures of WIN compounds bound to HRV14 were first determined, ligand

binding was reported to be associated with a significant conformational change. Residues at the carboxyl end of the *GH* loop and the start of the *H* strand of the VP1 β-barrel appeared to be collapsed into the mouth of the binding pocket when the pocket was vacant and forced by steric effects further out into the interface between fivefold-related protomers when the pocket was filled (Smith *et al.*, 1986, Kim *et al.*, 1993). These observations suggested a causative connection between the drug-induced conformational change and the drug-induced stabilization of virus against thermal denaturation and against the receptor-induced uncoating transition. Although such a possibility still cannot be ruled out, the drug-binding studies in poliovirus (Grant *et al.*, 1994) and rhinoviruses 16 and 1A (Oliveira *et al.*, 1993; Kim *et al.*, 1989) demonstrate conclusively that no such conformational change is necessarily required. In the present study, for example, all of the features in the difference map which correspond to changes in the protein correspond to fairly subtle conformational alterations, yet P3/Sabin, which changes little, is a better target for WIN51711 than HRV14, which changes significantly.

Assuming that large conformational adjustments in the virus are not required for this class of drug to be effective, the mechanism of stabilization must have an alternative explanation. In the absence of a ligand, the hydrophobic core of the β-barrel of VP1 would be very poorly packed. This would be expected to result in increased flexibility and compressibility of VP1. The poor packing could permit or induce shifts in several regions of the surrounding protein, including the *GH* and *EF* loops which shift upon ligand binding in rhinovirus 14. Indeed, the shifts may be even larger than those observed in rhinovirus 14, since the drug-binding pocket in the native rhinovirus 14 structure is not truly empty, but rather is occupied by four buried solvent molecules. Either shifts or increased flexibility could destabilize the virus by weakening intersubunit interactions in critical interfaces.

An increasing body of genetic evidence implicates the lipid-binding pocket in the regulation of poliovirus stability. This suggests that the drug simply may be playing an extreme version of the regulatory role normally played by the natural ligand in the viral life cycle. Thus, the antiviral and stabilizing effects of the drugs are direct effects of the ability of the drugs to fill the binding pocket more completely than the natural ligand does. This results in a greater affinity of the site for the drug, relative to the natural ligand, and greater difficulty in displacing the drug upon receptor binding or exposure to elevated temperature.

This work was supported by an NIH grants AI30580 and AI32480 (to JMH). The authors would like to thank Drs Mark McKinlay and Dan Pevear of Sterling-Winthrop for the gift of WIN51711.

References

AL-NAKIB, W., HIGGINS, P. G., BARROW, G. I., TYRRELL, D. A. G., ANDRIES, K., VANDEN BUSSCHE, G., TAYLOR, N. & JANSSEN, P. A. J. (1989). *Antimicrob. Agents Chemother.* **33**, 522–525.

ANDRIES, K., DEWINDT, B., SNOEKS, J., WILLEBRORDS, R., VAN EEMEREN, K., STOKBROEKX, R. & JANSSEN, P. A. J. (1992). *Antimicrob. Agents Chemother.* **36**, 100–107.

ANDRIES, K., DEWINDT, B., SNOEKS, J., WOUTERS, J., MOEREELS, H., LEWI, P. J. & JANSSEN, P. A. (1990). *J. Virol.* **64**(3), 1117–1123.

BADGER, J., KRISHNASWAMY, S., KREMER, M. J., OLIVEIRA, M. A., ROSSMANN, M. G., HEINZ, B. A., RUECKERT, R. R., DUTKO, F. J. & MCKINLAY, M. A. (1989). *J. Mol. Biol.* **207**, 163–174.

BADGER, J., MINOR, I., KREMER, M. J., OLIVEIRA, M. A., SMITH, T. J., GRIFFITH, J. P., GUERIN, D. M. A., KRISHNASWAMY, S., LUO, M., ROSSMANN, M. G., MCKINLAY, M. A., DIANA, G. D., DUTKO, F. J., FANCHER, M., RUECKERT, R. R. & HEINZ, B. A. (1988). *Proc. Natl Acad. Sci. USA*, **85**, 3304–3308.

BADGER, J., MINOR, I., OLIVEIRA, M. A., SMITH, T. J. & ROSSMANN, M. G. (1989). *Proteins*, **6**, 1–19.

BALTIMORE, D., GIRARD, M. & DARNELL, J. E. (1966). *Virology*, **29**, 179–189.

BASAVAPPA, R., SYED, R., FILMAN, D. J., ICENOGLE, J. P., FLORE, O. & HOGLE, J. M. (1994). *Protein Sci.* **3**, 1651–1699.

BERNSTEIN, F. C., KOETZLE, T. F., WILLIAMS, G. J. B., MEYER, E. G. JR, BRICE, M. D., RODGERS, J. R., KENNARD, O., SHIMANOUCHI, T. & TASUMI, M. (1977). *J. Mol. Biol.* **112**, 535–542.

BRICOGNE, G. (1974). *Acta Cryst.* A**30**, 395–405.

BRÜNGER, A. T., KURIYAN, J. & KARPLUS, M. (1987). *Science*, **235**, 458–460.

CALIGUIRI, L. A., MCSHARRY, J. J. & LAWRENCE, G. W. (1980). *Virology*, **105**, 86–93.

DIANA, G. D., CUTLIFFE, D., OGLESBY, R. C., OTTO, M. J., MALLAMO, J. P., AKULLIAN, V. & MCKINLAY, M. A. (1989). *J. Med. Chem.* **32**, 450–455.

DORVAL, B. L., CHOW, M. & KLIBANOV, A. M. (1990). *Biotechnol. Bioeng.* **35**, 1051–1054.

FILMAN, D. J., SYED, R., CHOW, M., MACADAM, A. J., MINOR, P. D. & HOGLE, J. M. (1989). *EMBO J.* **8**, 1567–1579.

FLORE, O., FRICKS, C. E., FILMAN, D. J. & HOGLE, J. M. (1990). *Semin. Virology*, **1**, 429–438.

FOX, M. P., OTTO, M. J. & MCKINLAY, M. A. (1986). *Antimicrob. Agents Chemother.* **30**, 110–116.

FRICKS, C. E. & HOGLE, J. M. (1990). *J. Virol.* **64**, 1934–1945.

GRANT, R. A., FILMAN, D. J., FUJINAMI, R. S., ICENOGLE, J. P. & HOGLE, J. M. (1992). *Proc. Natl Acad. Sci. USA*, **89**, 2061–2065.

GRANT, R. A., HIREMATH, C. N., FILMAN, D. J., SYED, R., ANDRIES, K. & HOGLE, J. M. (1994). *Curr. Biol.* **4**(9). 784–797.

HOGLE, J., CHOW, M. & FILMAN, D. J. (1985). *Science*, **229**, 1359–1365.

HUMMLER, K. ANDERSON, T. F. & BROWN, R. A. (1962). *Virology*, **16**, 84–90.

ISMAIL-CASSIM, N., CHEZZI, C. & NEWMAN, J. F. E. (1990). *J. Gen. Virol.* **71**, 2283–2289.

JACOBSON, D., HOGLE, J. M. & FILMAN, D. J. (1995). In preparation.

JONES, T. A. (1978). *J. Appl Cryst.* **11**, 268–272.

KATAGIRI, S. HINUMA, Y. & ISHIDA, N. (1967). *Virology*, **34**, 797–799.

KIM, S., SMITH, T. J., CHAPMAN, M. S., ROSSMANN, M. G., PEVEAR, D. C., DUTKO, F. J., FELOCK, P. J., DIANA, G. D. & MCKINLAY, M. A. (1989). *J. Mol. Biol.* **210**, 91–111.

KIM, K. H., WILLINGMANN, P., GONG, Z. X., KREMER, M. J., CHAPMAN, M. S., MINOR, I., OLIVEIRA, M. A., ROSSMANN, M. G., ANDRIES, K., DIANA, G. D., DUTKO, F. J., MCKINLAY, M. A. & PEVEAR, D. C. (1993). *J. Mol. Biol.* **230**, 206–227.

LEBOUVIER, G. L. (1959). *Br. J. Exp Pathol.* **40**, 605–620.

MACADAM, A. J., FERGUSON, G., ARNOLD, C. & MINOR, P. D. (1991). *J. Virol.* **65**, 5225–5231.

MCSHARRY, J. J., CALIGUIRI, L. A. & EGGERS, H. J. (1979). *Virology*, **97**, 307–315.

MOSSER, A. G. & RUECKERT, R. R. (1993). *J. Virol.* **67**(3), 1246–1254.

MOSSER, A. G., SGRO, J.-Y. & RUECKERT, R. R. (1995). *J. Virol.* In the press.

OLIVEIRA, M. A., ZHAO, R., LEE,W.-M., KREMER, M. J., MINOR, I., RUECKERT, R. R., DIANA, G. D., PEVEAR, D. C., DUTKO, F. J., MCKINLAY, M. A. & ROSSMANN, M. G. (1993). *Structure*, **1**, 51–68.

PEVEAR, D. C., FANCHER, M. J., FELOCK, P. J., ROSSMANN, M. G., MILLER, M. S., DIANA, G., TREASURYWALA, A. M., MCKINLAY, M. A. & DUTKO, F. J. (1989). *J. Virol.* **63**, 2002–2007.

ROIZMAN, B., MAYER, M. M. & ROANE, P. R. (1959). *J. Immunol.* **82**, 19–25.

ROSSMANN, M. G., ARNOLD, E., ERICKSON, J. W., FRANKENBERGER, E. A., GRIFFTH, J. P., HECHT, H. J., JOHNSON, J. E., KAMER, G., LUO, M., MOSSER, A. G., RUECKERT, R. R., SHERRY, B. & VRIEND, G. (1985). *Nature* (*London*), **317**, 145–153.

SMITH, T. J., KREMER, M. J., LUO, M., VRIEND, G., ARNOLD, E., KAMER, G., ROSSMANN, M. G., MCKINLAY, M. A., DIANA, G. D. & OTTO, M. J. (1986). *Science*, **233**, 1286–1293.

WALLIS, C. & MELNICK, J. L. (1961). *Tex. Rep. Biol. Med.* **19**, 683–700.

WINKLER, F. K., SCHUTT, C. E. & HARRISON, S. C. (1979). *Acta Cryst.* **35**, 901–911.

WOODS, M. G., DIANA, G. D., ROGGE, M. C., OTTO, M. J., DUTKO, F. J. & MCKINLAY, M. A. (1989). *Antimicrob. Agents Chemother.* **33**, 2069–2074.

YEATES, T. O., JACOBSON, D. H., MARTIN, A., WYCHOWSKI, C., GIRARD, M., FILMAN, D. J. & HOGLE, J. M. (1991). *EMBO J.* **10**, 2331–2341.